HTML ABSTRACT + LINKS

Properties of As^+-implanted and annealed GaAs and InGaAs quantum wells: Structural and band-structure modifications

J. W. Tomm,[a] V. Strelchuk,[b] and A. Gerhardt
Max-Born-Institut für Nichtlineare Optik und Kurzzeitspektroskopie, Max-Born-Str. 2 A, 12489 Berlin, Germany

U. Zeimer, M. Zorn, H. Kissel, and M. Weyers
Ferdinand-Braun-Institut für Höchstfrequenztechnik, Albert-Einstein-Str. 11, 12489 Berlin, Germany

J. Jiménez
Universidad de Valladolid, Fisica de la Materia Condensada, ETSII, 47011 Valladolid, Spain

(Received 29 September 2003; accepted 10 November 2003)

Both crystal structure and energy band-structure changes caused by As^+ implantation and by subsequent annealing in GaAs and in an $In_{0.253}Ga_{0.747}As$ quantum well are studied. We demonstrate that the main implantation impact to the crystal structure is the creation of a large number of point defects and strong compressive strain of up to -0.1%. Raman and x-ray data demonstrate almost complete structural recovery for rapid thermal annealing temperatures$\geqslant 600\,^{\circ}C$. While the lattice expansion becomes relaxed by annealing, the implantation-induced ionized point defects are still present up to the highest annealing temperatures applied. Under these circumstances, a 22 meV blueshift of the heavy-hole–electron (1hh–1e) transition within the quantum well and a substantial reduction of the nonequilibrium carrier lifetime remain as consequence of implantation. © *2004 American Institute of Physics.* [DOI: 10.1063/1.1637956]

I. INTRODUCTION

Ion implantation is one basic technique in solid-state technology, which is used in mass production for several purposes, such as post-growth doping, creation of insulating layers, and carrier-pair-lifetime engineering. There are several studies that employ, among others, Raman spectroscopy for studying the impact of implantation and, to some extent, subsequent annealing. These reports reveal at least one common experimental fact: Ion implantation causes a *low-energy shift* of the phonon Raman lines that may be compensated, depending on the conditions chosen, either in part or almost completely by annealing. The presence of the low-energy shift is independent of implantation doses, energies, and the species that is implanted (e.g., O,[1] Si,[2] Ar,[3] Be,[4] As,[5] P,[6] and H[7]); only its magnitude is governed by these parameters. The following interpretations for the shift are suggested: (i) tensile strain, which is well-known to reduce phonon energies[8] (cf. Si[9] or GaAs[7,10]). (ii) anharmonicity in the vibrational potential according to the explanations outlined in Refs. 6 and 11, and (iii) phonon confinement (''spatial correlation model''). The finite size of regions that are assumed to be formed during implantation hinder the free propagation of phonons, resulting in a range of allowed q values out of the zone center. According to the analysis suggested by Tiong *et al.*[5] (see also references therein), one obtains a localization length that is attributed to the diameter of unperturbed crystalline areas or a ''grain size'' that corresponds to the spatial correlation length.

The idea underlying our study is to combine a Raman study with careful monitoring of both structural and band-structure changes caused by implantation and subsequent annealing. For crosschecking the results on GaAs, we have buried an additional ''sensor'' into our GaAs sample; namely, an $In_{0.253}Ga_{0.747}As$ quantum well (QW). As^+-ion energy and dose are chosen such that both GaAs cladding and $In_{0.253}Ga_{0.747}As$ are impacted by the implantation process in almost the same way. Besides Raman spectroscopy, the samples are studied by diverse analytical tools, such as high-resolution x-ray diffraction (HRXRD), cathodoluminescence (CL), photocurrent (PC), and low-temperature, steady-state, and time-resolved photoluminescence (PL).

From complementary analysis of the results, it turns out that the expansion of the crystal lattice due to implantation recovers after appropriate annealing procedures, whereas the electronic structure remains smeared out by a high concentration of defects.

II. EXPERIMENTAL PROCEDURE

The layer sequence of the samples used in this study consists of a 180-nm-thick GaAs buffer layer, a 9.5-nm-thick, compressively strained $In_{0.253}Ga_{0.747}As$ QW ($\varepsilon = -1.812\%$), and a 66-nm-thick GaAs cladding layer. The layers were grown by metalorganic vapor-phase epitaxy on an exactly (001)-oriented GaAs 2 in. wafer. After epitaxy, half a wafer was implanted with 150 keV As^+ ions with a dose of $3.5\times 10^{12}\ cm^{-2}$. The implanted wafer part was cleaved into several $10\times 10\ mm^2$ pieces that experienced a rapid thermal annealing (RTA) process for 60 s at different temperatures (T_{RTA}) ranging from 400 to 650 °C. Thus, the RTA temperature is the main parameter in our study.

[a]Electronic mail: tomm@mbi-berlin.de
[b]Institute of Semiconductor Physics, National Academy of Sciences, Prospect Nauki 45, 252650 Kiev, Ukraine.

 © 2004 American Institute of Physics

Downloaded 30 Jan 2004 to 62.141.181.225. Redistribution subject to AIP license or copyright, see http://jap.aip.org/jap/copyright.jsp

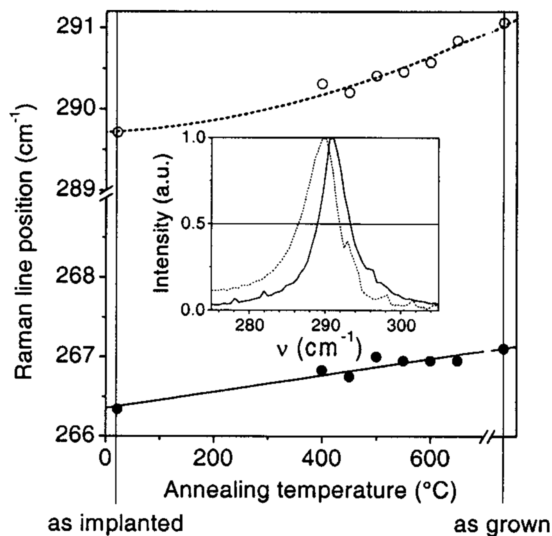

FIG. 1. Spectral position of the Γ-point LO- and TO-phonon peaks arising from the GaAs-like modes from both the bulk-like GaAs as well as from the QW versus RTA temperature. Data from the as-grown sample are shown at the right, behind the axis break of the abscissa. Data from the as-implanted sample are presented at ambient temperature. The inset gives LO-phonon peaks for the as grown (full line) and as-implanted samples (dotted line).

Room-temperature Raman spectra are recorded in backscattering geometry using a $f=0.6$ m DILOR spectrometer after excitation by an argon-ion laser emitting at 514.5 nm. The exciting laser beam ($P=850$ μW) that is directed parallel to the growth direction is focused by a microscope objective (×50) onto the sample, resulting in a ~1-μm-diameter spot. The backscattered light is detected with a LN_2-cooled Si CCD camera. PC spectra are recorded by a BRUKER IFS 66v Fourier transform infrared spectrometer for in-plane excitation; that is, perpendicular to the growth direction. Contact pads are mechanically fixed on cladding and substrate of the structure. The HRXRD measurements are carried out using a Philips MRD equipped with a Barthels monochromator and a 0.75 mm slit in front of the detector. The obtained $\Omega/2\Theta$ rocking curves are fitted using the EPITAXY4 software. The fitting model provides the layer thicknesses of the GaAs cladding layer and the InGaAs QW, as well as the indium concentration and the additional strain after implantation and annealing. Time-resolved PL is performed by using a Tsunami Ti:sapphire laser for the creation of sub-100-fs excitation pulses (repetition rate 82 MHz, wavelength 785 nm). Detection is done by a Hamamatsu synchroscan streak camera with IR-enhanced cathode. The overall temporal resolution of the complete setup is about 10 ps.

III. RESULTS

Raman data (i.e., the Γ-point TO- and LO-phonon peak positions) versus T_{RTA} are shown in Fig. 1. These lines arise from the GaAs-like modes from both the bulk-like GaAs as well as from the QW. Contributions from the InAs-like modes of the QW, expected in the 230–240 cm^{-1} range, are not detected. In this figure, as well in all following ones in which we present data versus RTA temperature, we place the data from the as-implanted samples at ambient temperature,

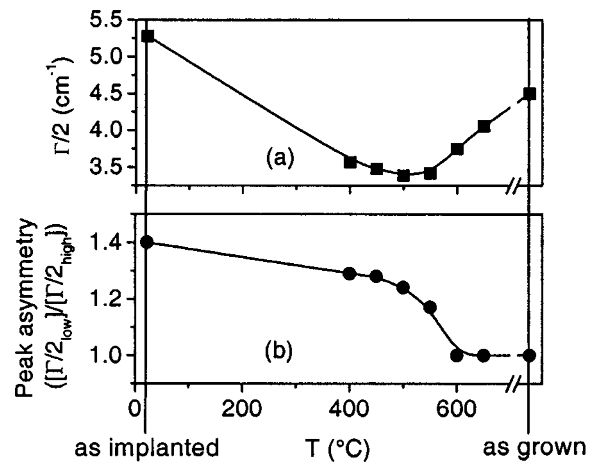

FIG. 2. Raman line-shape analysis. (a) FWHM Γ/2 of the LO-phonon peaks versus RTA temperature. (b) Peak asymmetry of the LO-phonon peaks versus RTA temperature.

whereas the data from the as-grown sample are arranged after an axis break at the high-temperature end of the T_{RTA} scale. As described in the introduction, the Raman lines experience a low-energy shift after implantation, which is partly removed by annealing. The inset shows the LO-type lines of the as-grown and as-implanted samples, demonstrating the spectral shift as well as the asymmetric line broadening after implantation.

Results of detailed Raman line-shape analysis are summarized in Fig. 2. In Fig. 2(a), we show the full width at half-maximum (FWHM) (Γ/2), whereas Fig. 2(b) illustrates the "Raman peak asymmetry" by giving the ratio $(\Gamma/2_{low})/(\Gamma/2_{high})$. $(\Gamma/2_{low})$ and $(\Gamma/2_{high})$ represent the shift between the line center and the low- and high-energy wing of the spectra, respectively, with $(\Gamma/2)=(\Gamma/2_{low})+(\Gamma/2_{high})$. Both sets of data are plotted versus T_{RTA}, where the data for the "as implanted" and "as grown" samples are again arranged as described for Fig. 1. We complete the presentation of Raman data by providing excitation-power-dependent Raman data for two samples in Fig. 3. Both samples exhibit a very different evolution of Γ/2 with increasing excitation density.

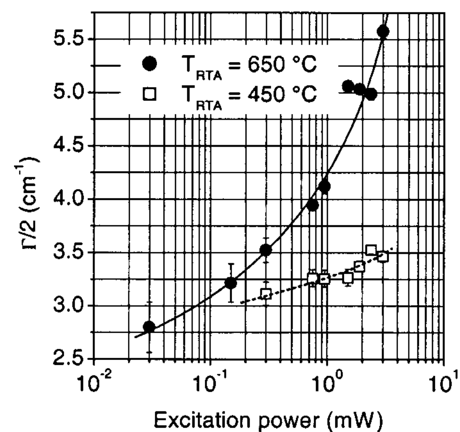

FIG. 3. FWHM of LO-phonon peaks versus excitation power for the samples that experienced RTA at 450 and 650 °C. The standard power used in the Raman experiments is 850 μW.

Downloaded 30 Jan 2004 to 62.141.181.225. Redistribution subject to AIP license or copyright, see http://jap.aip.org/jap/copyright.jsp

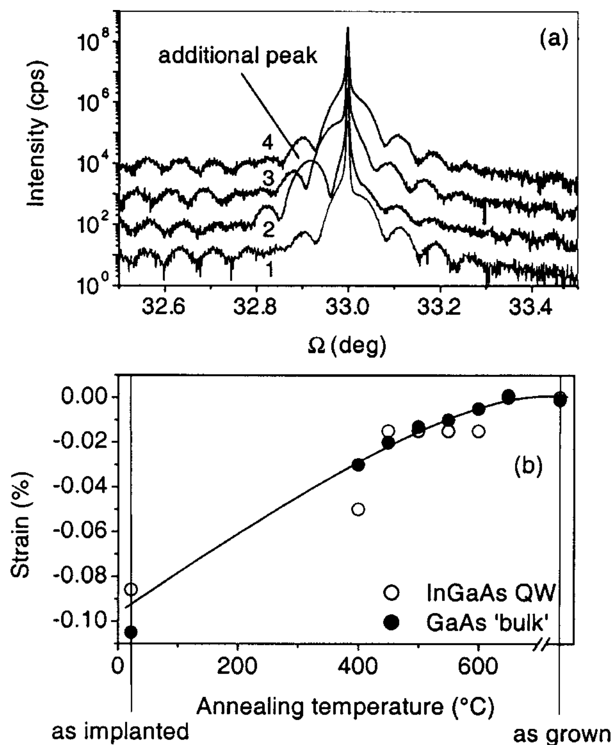

FIG. 4. (a) HRXRD rocking curves from the as-grown (1), as-implanted (2), and from the samples annealed at $T_{RTA}=400\,°C$ (3) and 650 °C (4). (b) Deformation of the GaAs cladding (full circles) and the $In_{0.253}Ga_{0.747}As$ QW (open circles) obtained by modeling of HRXRD rocking curves. The built-in strain $\varepsilon=-1.812\%$ of the $In_{0.253}Ga_{0.747}As$ QW on GaAs was set to zero for this display.

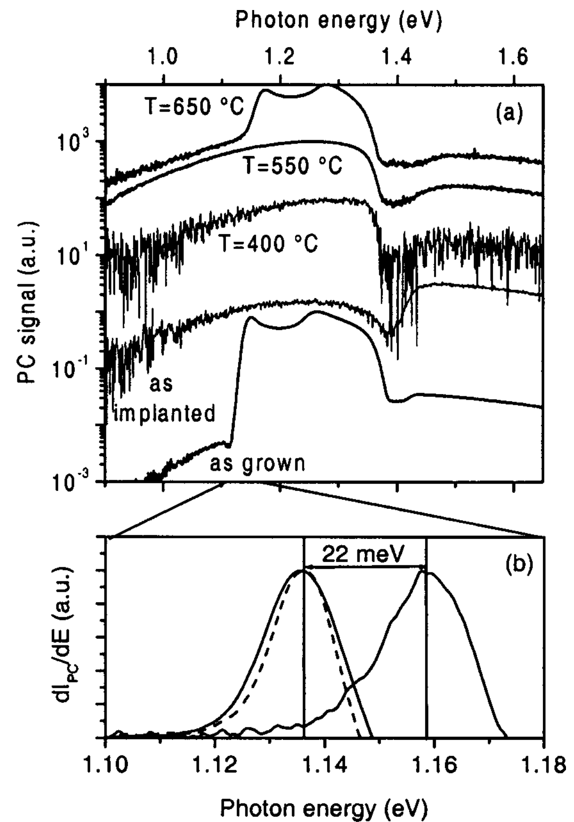

FIG. 5. (a) RT PC spectra of the as-grown, as-implanted, and implanted and annealed ($T_{RTA}=400$, 550, and 650 °C) samples. The main structure at 1.136 eV is caused by the 1hh–1e optical transition in the $In_{0.253}Ga_{0.747}As$ QW. The spectra are shifted against each other by multiplying the data with constant factors. (b) Normalized first derivatives of the spectra (dI_{PC}/dE) in the range of the 1hh–1e optical transition in the $In_{0.253}Ga_{0.747}As$ QW. The full lines show the 1hh–1e resonance for the as-grown at 1.136 eV and the implanted sample with $T_{RTA}=650\,°C$ at 1.158 meV. The dashed line representing data from an nonimplanted sample that experienced RTA at 650 °C is added for reference. The absolute value of dI_{PC}/dE for the as-grown sample exceeds the one of the as-implanted sample by a factor of 10.

HRXRD rocking curves for as-grown and as-implanted samples, as well as for samples annealed at 450 and 650 °C, are shown in Fig. 4(a). The implantation impact is seen as an additional peak at the low-angle side of the substrate peak, indicating a region with additional compressive strain. This indicates, in fact, the GaAs cladding layer has a higher lattice parameter after implantation due to the formation of Frenkel defects.[12] The InGaAs peak (not shown here) is shifted to lower angles as well. Obviously, both the 9.5-nm-thick QW and the 66 nm GaAs cladding are impacted by the technological processes by almost the same amount, as shown by detailed analysis for all T_{RTA} [cf. Fig. 4(b)]. For better comparability the $\varepsilon=-1.812\%$ built-in strain of the $In_{0.253}Ga_{0.747}As$ QW on GaAs was set to zero. The higher the annealing temperature, the more the implantation-induced compressive strain is reduced. For both the GaAs cladding layer and the InGaAs QW, this process takes place in the same way, and the additional strain is removed at an annealing temperature of 600 °C.

While Figs. 1–4 relate mainly to changes of the *structural properties* of the samples after implantation and subsequent annealing in the following the changes of the *electronic band structure* are addressed.

Figure 5(a) shows PC spectra, which characterize the absorption properties of the structure. Figure 5(b) shows selected first derivatives of the PC spectra in the QW-edge region. The full lines show the resonance created by the optical transition from the first heavy hole to the first electron state in the QW [heavy-hole–electron (1hh–1e)] for the as-grown at 1.136 eV and the implanted sample annealed at $T_{RTA}=650\,°C$ at 1.158 eV. The dashed line represents data from a nonimplanted sample that also experienced RTA at 650 °C. Thus, the whole 22 meV blueshift is considered implantation-induced.

Further information on the impact of the process to the electronic band structure was obtained from low-temperature PL. Spectra from the as-grown structure show a distinct excitonic QW emission at 1.221 eV ($T=10$ K), whereas all implanted samples show wide, infrared PL bands that are assigned to optical transitions involving deep levels. At the original QW emission energy a weak and broad emission band remains, which merges with the deep-level contributions. A general tendency of increased PL intensity with increasing RTA temperature is observed; however, even for the implanted sample with $T_{RTA}=650\,°C$, no return to a PL behavior being indicative for a QW is observed. The PL behavior is still dominated by defects.

Time-resolved PL ($T=10$ K) after impulsive femtosecond excitation, detected at the spectral position of the edge emission (1.221 eV), revealed luminescence decay times

Downloaded 30 Jan 2004 to 62.141.181.225. Redistribution subject to AIP license or copyright, see http://jap.aip.org/jap/copyright.jsp

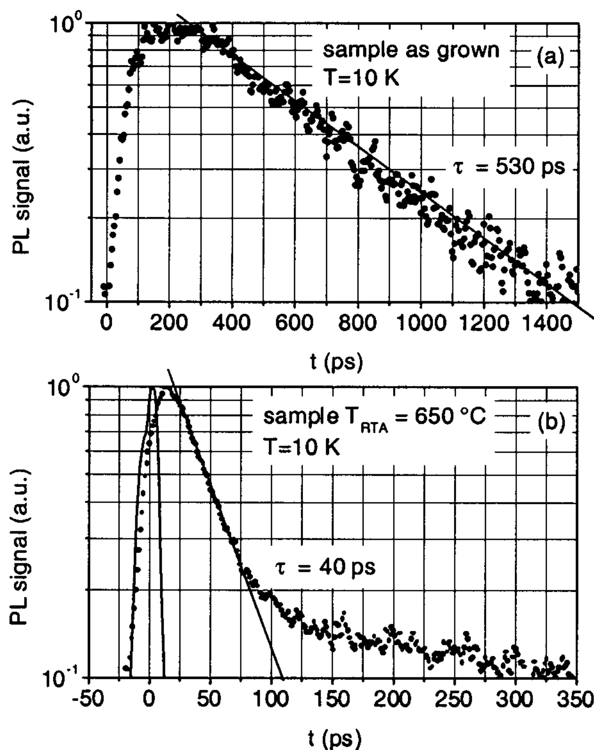

FIG. 6. Transient PL (T=10 K) after impulsive femtosecond excitation, detected at the spectral position of the edge emission (1.221 eV) for the as-grown (a) and the implanted sample that experienced RTA at 650 °C (b).

(~nonequilibrium carrier pair lifetimes) of 530 ps for the as-grown and 40 ps for the implanted sample that experienced RTA at 650 °C [Figs. 6(a) and 6(b)]. Samples annealed at lower T_{RTA} do not show any signal for this excitation regime confirming the presence of implantation-induced point defects, which act as traps for carriers killing any luminescence for samples experiencing lower T_{RTA}. Obviously, the traps are subsequently removed during RTA, but only in part, even at temperatures as high as $T_{RTA}=650$ °C.

Panchromatic CL images show no significant change of the observed dark spot defect distribution for the as-grown sample with implantation. The implantation, however, causes a substantial decrease of the CL intensity. Thus, homogeneously distributed point defects seem to be the only effect of implantation. In addition, RTA does not generate any local defect accumulations that result in a notable additional CL contrast.

IV. DISCUSSION

We start the discussion by analyzing the data describing the structural changes of the sample after implantation and RTA. The Raman data in Fig. 1 show the LO line shift of 1.4 cm^{-1} between as-grown and as-implanted sample to be more pronounced compared to the TO line shift of 0.7 cm^{-1}. This agrees well with the "spatial correlation model" due to the weaker dispersion of the TO phonons compared to the LO at the Γ point. The LO line shift indicates a grain size of slightly less than 10 nm (cf. Ref. 5) for the areas in which translation symmetry after implantation is still maintained. The Raman bands are clearly asymmetrical for as-implanted samples and samples annealed below 550 °C. According to the spatial correlation model (cf. Ref. 13), this asymmetry also allows to estimate the grain size. We find a value of 8–10 nm. This is in good agreement with the numbers obtained from the shift. The peak symmetry is improved for increasing annealing temperature, reaching a symmetric shape at 600 °C. This means that the translation symmetry is restored at that temperature. This result is in excellent agreement with the results of the relaxation of the lattice constant obtained by HRXRD (cf. Fig. 4). The Γ/2 data additionally confirm this interpretation by showing a substantial reduction, at least up to RTA temperatures of 500–550 °C.

The increase of the Γ/2 towards even higher RTA temperatures is most likely due to another effect that will be outlined in the following. The LO Raman band involves contributions of free carriers, which, for concentrations below 10^{17} cm^{-3}, can induce a broadening of the LO phonon band. Hence, the LO line should be considered rather as a combination of a regular LO phonon band and the L^+ branch of the longitudinal optic plasmon coupled (LOPC) mode. In as-grown samples, the density of defects is very low and the lifetime high (cf. time-resolved PL data given in Fig. 6). The Raman microprobe can generate the steady-state free carrier concentration necessary to broaden the LO band by a substantial LOPC contribution. In the implanted and annealed samples, the lifetime of the generated carriers is governed by the recombination at crystal defects (traps) reducing the carrier lifetime and thus, the steady-state free carrier concentration. That in turn lowers the LOPC contribution to the LO band broadening. Figure 3 confirms this by demonstrating the substantially stronger excitation power sensitivity of Γ/2 for the sample that experienced RTA at a higher temperature and for which, consequently, a higher steady-state nonequilibrium carrier concentration during the Raman measurement is to be expected. Note that this discussion is consistent with the time-resolved PL data; Fig. 6 provides evidence of significant changes in the lifetime of nonequilibrium carriers during annealing. Furthermore, the Raman data is consistent with the HRXRD results as well, which demonstrate almost complete recovery of the lattice constants at $T_{RTA}=600$ °C.

While the strain caused by point defects is removed by annealing, they still affect the band structure. Considering the PC data, we find, for the as-grown sample, a pronounced QW absorption edge that becomes annihilated by ion implantation, but which is subsequently restored again by RTA [Fig. 5(a)]. From an analysis of the first derivatives of the PC spectra, we find the 1hh–1e resonance for the as-grown sample at at 1.136 eV and for the implanted sample with $T_{RTA}=650$ °C at 1.158 eV [Fig. 5(b)]. The resonance of an nonimplanted reference sample that also experienced RTA at 650 °C remains unshifted. Thus, the shift is not due to RTA-induced QW intermixing, and the whole 22 meV blueshift is considered implantation induced. Assuming, tentatively, this shift to be caused by hydrostatic compressive strain, we would find a corresponding strain of about −0.1%. Assuming, alternatively, a deformation of the QW for the present QW structure, a 22 meV blueshift would correspond to a lowering of the mole fraction x by 0.025 or a narrowing of the QW width by 2.6 nm. Both assumptions clearly contra-

Downloaded 30 Jan 2004 to 62.141.181.225. Redistribution subject to AIP license or copyright, see http://jap.aip.org/jap/copyright.jsp

dict the HRXRD data (cf. Fig. 4). Note that, in particular, the similar behavior of the QW and GaAs bulk seen in Fig. 4(b) clearly contradicts the assumption of a change in QW shape. Nevertheless, a substantial change of QW properties is clearly shown by the PC data as well as by the lifetime reduction (Fig. 6). By taking the difference between the photocurrents created by the defect band (at 1.11 eV) and the QW (at 1.16 eV) [cf. Fig. 5(a) bottom and top], we find a ratio between the deep-level defect concentrations of the as-grown and the implanted sample with $T_{RTA}=650\,^{\circ}C$ of >25. This conservative estimation (neglecting PC saturation) visualizes that, assuming a typical background concentration of 10^{17} cm^{-3} for the as-grown sample [cf. discussion of Figs. 2(a) and 3], a carrier and defect concentration of more than 10^{18} cm^{-3} for the implanted sample with $T_{RTA}=650\,^{\circ}C$ is a realistic value. As has been pointed out in Ref. 12, the concentration of interstitials and vacancies has to be below 10^{19} cm^{-3} for not causing a change of the lattice parameter. Thus, the actual carrier concentration after annealing at $T_{RTA}=650\,^{\circ}C$ is expected on the order of several 10^{18} cm^{-3}. This estimation is additionally supported by the absence of any pronounced excitonic features in low-temperature, steady-state PL and the predominance of deep-level-related emission, even for the implanted sample with $T_{RTA}=650\,^{\circ}C$. This concentration of ionized defects and free carriers explains well both lifetime reduction by trapping as well as the blueshift of the PC resonance. The microscopic nature of the latter one is assumed to be caused by the presence of a large concentration of localized charged ions (QW potential degradation) and/or a Burstein–Moss shift of the QW edge (absence of the lowest quantum-confined transitions in absorption and consequently also in PC), which is caused by the increased carrier concentration.

V. SUMMARY

We simultaneously monitor changes in crystal structure and band structure caused by As^{+} implantation (energy: 150 keV; fluence: 3.5×10^{12} cm^{-2}) and subsequent annealing in GaAs and in an $In_{0.253}Ga_{0.747}As$ QW.

The Raman spectra after implantation exhibit a low-energy shift of the LO- and TO-phonon lines arising from the GaAs-like modes from both the bulk-like GaAs as well as from the QW and an increased asymmetry. The shift, as well as the asymmetry, is reduced by RTA. From the lattice constant changes measured by HRXRD, it becomes clear that these Raman shifts are not caused by tensile strain. The spatial correlation model, however, provides concordant quantitative explanations for both the shift and the observed line-shape changes of the phonon peaks.

We demonstrate that the main implantation impact to the crystal structure is the creation of a large number of point defects and strong compressive strain of up to -0.1% within both GaAs and QW. Both Raman and HRXRD data show almost complete recovery of the lattice parameters for $T_{RTA}=600\,^{\circ}C$ and higher. While the compressive strain becomes relaxed by RTA, the implantation-induced ionized point defects are still present up to $T_{RTA}=650\,^{\circ}C$. These defects and the free carriers caused by their ionization modify the QW absorption, in particular the PC spectrum, resulting in a 22 meV shift of the 1hh–1e transition, and substantially reduce the nonequilibrium carrier lifetime to less than 10% of the initial value.

ACKNOWLEDGMENT

The authors would like to thank G. Schöne for ion implantation and Dr. R. Lossy for the annealing of the samples.

[1] H. Yamazaki and K. Watanabe, Appl. Phys. Lett. **64**, 2540 (1994).
[2] M. Holz, R. Zallen, A. E. Geissberger, and R. Sadler, J. Appl. Phys. **59**, 1946 (1986).
[3] J. Wagner and Ch. Hoffman, Appl. Phys. Lett. **50**, 682 (1987).
[4] M. Holz, R. Zallen, O. Brafman, and S. Matteson, Phys. Rev. B **37**, 4609 (1988).
[5] K. K. Tiong, P. M. Amirtharaj, and F. H. Pollak, Appl. Phys. Lett. **44**, 122 (1984).
[6] P. Verma, S. C. Abbi, and K. P. Jain, Phys. Rev. B **51**, 16660 (1995).
[7] E. Anastassakis and J. Tatarkiewicz, Appl. Phys. Lett. **50**, 245 (1987).
[8] G. Landa, R. Carles, C. Fontaine, E. Bedel, and A. Munoz-Yagüe, J. Appl. Phys. **66**, 196 (1989).
[9] D. Olego, H. Baumgart, and G. K. Celler, Appl. Phys. Lett. **52**, 483 (1988).
[10] P. S. Pizani, A. Mlayah, J. Groenen, R. Carles, and A. Claverie, Appl. Phys. Lett. **66**, 1927 (1995).
[11] M. Balkanski, R. F. Wallis, and E. Haro, Phys. Rev. B **28**, 1928 (1983).
[12] U. Zeimer and E. Nebauer, Semicond. Sci. Technol. **15**, 965 (2000).
[13] P. Parayanthal and F. H. Pollak, Phys. Rev. Lett. **52**, 1822 (1984).

Downloaded 30 Jan 2004 to 62.141.181.225. Redistribution subject to AIP license or copyright, see http://jap.aip.org/jap/copyright.jsp